

# Comparative experimental and theoretical study on anomalous Nernst effect of Heusler alloy $\text{Co}_2\text{FeSi}$ thin film: estimation of on-site Coulomb interaction at Co site

Weinan Zhou, Keisuke Masuda, Kazuki Sumida, Yuichi Fujita, Akio Kimura & Yuya Sakuraba

**To cite this article:** Weinan Zhou, Keisuke Masuda, Kazuki Sumida, Yuichi Fujita, Akio Kimura & Yuya Sakuraba (2025) Comparative experimental and theoretical study on anomalous Nernst effect of Heusler alloy  $\text{Co}_2\text{FeSi}$  thin film: estimation of on-site Coulomb interaction at Co site, Science and Technology of Advanced Materials, 26:1, 2564061, DOI: 10.1080/14686996.2025.2564061

**To link to this article:** <https://doi.org/10.1080/14686996.2025.2564061>



© 2025 The Author(s). Published by National Institute for Materials Science in partnership with Taylor & Francis Group.



View supplementary material [↗](#)



Published online: 28 Oct 2025.



Submit your article to this journal [↗](#)



Article views: 462









View related articles [↗](#)



View Crossmark data [↗](#)

# Comparative experimental and theoretical study on anomalous Nernst effect of Heusler alloy $\text{Co}_2\text{FeSi}$ thin film: estimation of on-site Coulomb interaction at Co site

Weinan Zhou <sup>a</sup>, Keisuke Masuda <sup>a</sup>, Kazuki Sumida <sup>b</sup>, Yuichi Fujita <sup>a\*</sup>, Akio Kimura <sup>c,d,e</sup> and Yuya Sakuraba <sup>a</sup>

<sup>a</sup>Research Center for Magnetic and Spintronic Materials (CMSM), National Institute for Materials Science (NIMS), Tsukuba, Japan;

<sup>b</sup>Research Institute for Synchrotron Radiation Science, Hiroshima University, Higashi-Hiroshima, Japan;

<sup>c</sup>Graduate School of Advanced Science and Engineering, Hiroshima University, Higashi-Hiroshima, Japan;

<sup>d</sup>International Institute for Sustainability with Knotted Chiral Meta Matter (WPI-SKCM<sup>2</sup>), Hiroshima University, Higashi-Hiroshima, Japan;

<sup>e</sup>Synchrotron Radiation Research Center, National Institutes for Quantum Science and Technology (QST), Sayo, Japan

## ABSTRACT

$\text{Co}_2\text{FeSi}$  is considered a half-metallic ferromagnet and a Weyl semimetal, however, its predicted properties have been shown to be heavily influenced by how the on-site Coulomb interaction is incorporated, which remains controversial. In this study, we measure the anomalous Nernst conductivity ( $\alpha_{xy}$ ) and anisotropic magnetoresistance (AMR) effect of a  $\text{Co}_2\text{FeSi}$  thin film from low temperature to room temperature, and compare the results with those of first-principles calculations using different values for on-site Coulomb interaction at the Co site ( $U_{\text{Co}}$ ). Our measurements reveal that  $\alpha_{xy}$  is less than  $0.1 \text{ A m}^{-1} \text{ K}^{-1}$  at room temperature and decreases slightly with the temperature. The observed values of  $\alpha_{xy}$  are more than one order of magnitude smaller than the predictions unless a small but finite  $U_{\text{Co}}$  is incorporated. The AMR effect exhibits a notable sign change from negative to positive with increasing temperature, which is inconsistent with the predicted band structure calculated using a large  $U_{\text{Co}}$  value. By combining these experimental observations with first-principles calculations, we estimate that the appropriate  $U_{\text{Co}}$  value is approximately 1–2 eV. Our findings provide valuable insight into the correlation effect in  $\text{Co}_2\text{FeSi}$ , emphasizing the critical role of the on-site Coulomb interaction in accurately describing the transport properties of Co-based Heusler alloys.

## ARTICLE HISTORY

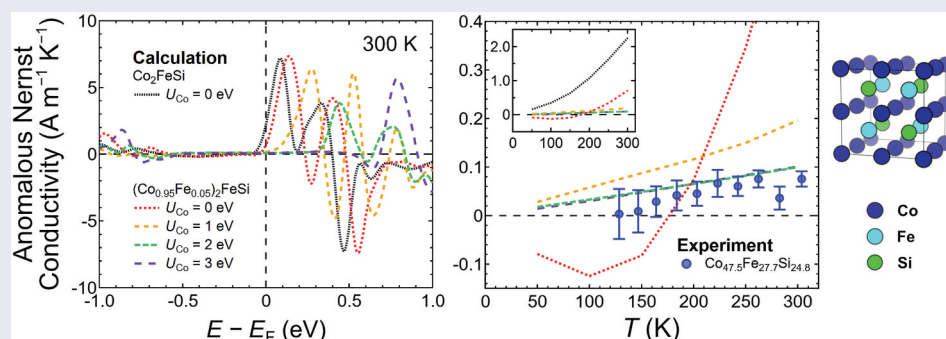
Received 25 April 2025

Accepted 17 September 2025

Revised 31 August 2025

## KEYWORDS

Heusler alloy;  $\text{Co}_2\text{FeSi}$ ; on-site Coulomb interaction; anomalous Nernst effect; anomalous Nernst conductivity; anisotropic magnetoresistance effect; anomalous Hall effect; temperature dependence





## IMPACT STATEMENT

Experimentally determined anomalous Nernst conductivity of  $\text{Co}_2\text{FeSi}$  agrees well with first-principles calculations when on-site Coulomb interaction at Co site is incorporated, thus provide valuable insights for materials exploration.


## 1. Introduction

Co-based Heusler alloys in the  $L2_1$  structure have attracted considerable interest in recent years because of their diverse and tunable properties. Many of these

alloys are predicted to exhibit half-metallicity, *i.e.*, a bandgap in one spin channel at the Fermi level ( $E_F$ ), resulting in 100% spin polarization [1–5]. This unique property significantly enhances magnetoresistance

**CONTACT** Weinan Zhou  [ZHOU.Weinan@nims.go.jp](mailto:ZHOU.Weinan@nims.go.jp); Yuya Sakuraba  [SAKURABA.Yuya@nims.go.jp](mailto:SAKURABA.Yuya@nims.go.jp)

\*Present address: Global Research and Development Center for Business by Quantum-AI technology (G-QuAT), National Institute of Advanced Industrial Science and Technology (AIST), Tsukuba, Ibaraki 305–8568, Japan.

 Supplemental data for this article can be accessed online at <https://doi.org/10.1080/14686996.2025.2564061>

© 2025 The Author(s). Published by National Institute for Materials Science in partnership with Taylor & Francis Group.

This is an Open Access article distributed under the terms of the Creative Commons Attribution License (<http://creativecommons.org/licenses/by/4.0/>), which permits unrestricted use, distribution, and reproduction in any medium, provided the original work is properly cited. The terms on which this article has been published allow the posting of the Accepted Manuscript in a repository by the author(s) or with their consent.

effects [6,7] and improves the efficiency of spin injection into nonmagnetic materials [8,9]. Exploiting this property has been a major approach for advancing the performance of spintronic devices such as magnetic sensors, magnetic random access memory (MRAM), nonlocal spin valves, and other related applications [10–12].

Meanwhile, it has been shown that some Co-based Heusler alloys can be classified as Weyl semimetals, possessing Weyl cones or nodal lines near  $E_F$  [13–17]. Such topologically nontrivial band structures induce large Berry curvature and are responsible for transport phenomena such as the large anomalous Hall effect (AHE) in  $\text{Co}_2\text{MnAl}$  [18] and large anomalous Nernst effect (ANE) in  $\text{Co}_2\text{MnGa}$  [17,19–21]. These features have inspired novel devices and functionalities leveraging these effects [10–12,22–24].

Among Heusler alloys,  $\text{Co}_2\text{FeSi}$  is a well-known and extensively studied material. Experiments on bulk  $\text{Co}_2\text{FeSi}$  have shown a notably high Curie temperature of approximately 1100 K and large magnetic moment of 6  $\mu_B/\text{f.u.}$  [25], which agrees with the magnetic moment for a half-metallic full-Heusler alloy predicted by the Slater-Pauling rule [3]. By contrast, first-principles calculations predicted smaller magnetic moments of approximately 5  $\mu_B/\text{f.u.}$  [25,26]. This discrepancy was addressed by incorporating the on-site Coulomb interaction ( $U$ ) in calculations. When assuming  $U$  values of 2.5–5.0 eV for the Co site and 2.5–4.5 eV for the Fe site, calculations not only yield a magnetic moment that is consistent with the experimental value but also exhibit a clear half-metallic energy gap in the minority-spin channel; while calculations show that  $\text{Co}_2\text{FeSi}$  is an ordinary ferromagnet rather than a half-metallic material if  $U$  is not taken into consideration [26,27]. However, experiments to determine the transport properties in relation to the half-metallicity of  $\text{Co}_2\text{FeSi}$  have produced mixed results. Magnetotransport measurements on a single crystal showed evidence for half-metallicity, as electron-magnon scattering was exponentially suppressed at low temperatures owing to gapped spin-flip scattering [28]. However, the experimentally extracted energy separation between  $E_F$  and the conduction band (CB) edge of the minority spin was significantly smaller than that predicted theoretically. The anisotropic magnetoresistance (AMR) effect was employed to study the half-metallicity of  $\text{Co}_2\text{FeSi}$ . According to the extended two-current model for AMR, which accounts for all  $s$ - $d$  electron scattering processes through different spin channels, a half-metallic material is expected to consistently exhibit a negative AMR ratio [29]. Notably, other half-metallic candidates such as  $\text{Co}_2\text{MnSi}$  and  $\text{Co}_2\text{FeGa}_{0.5}\text{Ge}_{0.5}$ , whose half-metallic nature has been demonstrated by tunneling magnetoresistance (TMR) [6] or current-perpendicular-to-

plane giant magnetoresistance (CPP-GMR) effect [7], have shown negative AMR ratios from low to room temperature, with minimal temperature dependence [30,31]. By contrast,  $\text{Co}_2\text{FeSi}$  exhibits a negative AMR ratio at low temperature and a positive ratio at room temperature, suggesting the collapse of its half-metallic nature as a result of thermal excitation [30]. Point-contact Andreev reflection spectroscopy measurements have indicated significantly lower spin polarization for  $\text{Co}_2\text{FeSi}$  than expected [32–35]. Furthermore, TMR and nonlocal spin valve devices using  $\text{Co}_2\text{FeSi}$  have shown results due to low spin polarization as well [36,37]. Consequently, the significance and necessity of incorporating  $U$  in describing  $\text{Co}_2\text{FeSi}$  remain controversial. Previously, Sumida *et al.* carried out resonant photoelectron spectroscopy measurements on a  $\text{Co}_2\text{FeSi}$  thin film and found that Fe 3d states existed approximately 2 and 4 eV below  $E_F$ , which was consistent with the calculated results without considering  $U$  at the Fe site [38]. Nevertheless, the impact of introducing  $U$  at the Co site appeared to be too subtle to produce observable changes when the experimental and calculated results were compared.

In this study, we investigated the impact of incorporating  $U$  at the Co site by measuring the anomalous Nernst conductivity ( $\alpha_{xy}$ ) of a  $\text{Co}_2\text{FeSi}$  thin film.  $\alpha_{xy}$  is closely linked to the Berry curvature of the electronic band structure and is particularly sensitive to the bands near  $E_F$ , in contrast to the anomalous Hall conductivity ( $\sigma_{xy}$ ), which accounts for contributions from all occupied bands [15,39]. Therefore,  $\alpha_{xy}$  has been used to study magnetic Weyl semimetals such as  $\text{Co}_2\text{MnGa}$  [17,19–21] and  $\text{Co}_3\text{Sn}_2\text{S}_2$  [40–42], along with other magnetic materials with topologically nontrivial band structures [43–47]. For  $\text{Co}_2\text{FeSi}$ , Noky *et al.* theoretically predicted large magnitude of  $\sigma_{xy}$  and  $\alpha_{xy}$  slightly above  $E_F$  without considering  $U$ , and identified the source of Berry curvature to be Weyl point [48]. The band structure of  $\text{Co}_2\text{FeSi}$  can be found in an earlier study by Huang *et al.* where the negative peak of  $\sigma_{xy}$  slightly above  $E_F$  can be attributable to multiple band crossings in the minority spin, mostly along the X – W direction [35]. The value of  $\alpha_{xy}$  for  $\text{Co}_2\text{FeSi}$  at  $E_F$  has been predicted to be 2.57  $\text{A m}^{-1} \text{K}^{-1}$  [48]. This is comparable to that for  $\text{Co}_2\text{MnGa}$ , which currently holds the record for the anomalous Nernst coefficient ( $S_{\text{ANE}}$ ) at room temperature [17,19–21]. However, no large  $S_{\text{ANE}}$  value for  $\text{Co}_2\text{FeSi}$  has yet been reported. Our experimental measurements revealed a significantly smaller  $\alpha_{xy}$  value of less than 0.1  $\text{A m}^{-1} \text{K}^{-1}$ , with small temperature dependence. By comparing these experimental findings with first-principles calculations employing various values for  $U$  at the Co site ( $U_{\text{Co}}$ ), we found good agreement between the experimental and theoretical results when a finite  $U_{\text{Co}}$  value larger than 1 eV was assumed.

Additionally, we measured the temperature dependence of the AMR effect using the same Co<sub>2</sub>FeSi thin film and observed a sign change from negative to positive with increasing temperature. This behavior contradicted the calculated band structures when assuming a  $U_{\text{Co}}$  value larger than 2 eV, thus providing an upper boundary. Collectively, these experimental results indicate that a small but finite value of  $U_{\text{Co}}$  is most appropriate for accurately describing Co<sub>2</sub>FeSi.

## 2. Methods

The Co<sub>2</sub>FeSi thin film was epitaxially grown on an MgO (100) single-crystal substrate via magnetron sputtering. The base pressure of the sputtering chamber was  $< 3 \times 10^{-6}$  Pa. Prior to deposition, the surface of the MgO substrate was cleaned by heating at 600°C for 30 min. Then, the Co<sub>2</sub>FeSi thin film was formed by the co-deposition of a Co<sub>50</sub>Fe<sub>25</sub>Si<sub>25</sub> alloy target and pure Si target. During the deposition, 120 W of DC power was supplied to the Co<sub>50</sub>Fe<sub>25</sub>Si<sub>25</sub> target, and 90 W of RF power was supplied to the Si target, under an Ar pressure of 0.9 Pa. The distance between the targets and substrate was  $\sim 25$  cm. The deposition was carried out for 27 min while maintaining the substrate temperature at 600°C. After the co-deposition, the sample was cooled to room temperature, followed by the deposition of a 2-nm-thick Al capping layer to prevent oxidation. To determine the composition, we used a quantitative application of an X-ray fluorescence (XRF; ZSX Primus II, Rigaku, Japan) analysis system, which was created by measuring multiple reference samples prepared in the laboratory. The compositions of these reference samples were determined using inductively coupled plasma mass spectroscopy. The composition and thickness of the Co<sub>2</sub>FeSi were Co<sub>47.5</sub>Fe<sub>27.7</sub>Si<sub>24.8</sub> and 41.7 nm, respectively. The deposition rate was estimated to be 0.26 Å s<sup>-1</sup>. The thin film structure was studied using X-ray diffraction (XRD; SmartLab, Rigaku, Japan) with Cu  $K_{\alpha}$  radiation. The magnetic properties were studied using a superconducting quantum interference device. To characterize the transport properties, the Co<sub>2</sub>FeSi thin film was patterned into a 2-mm-wide and 8-mm-long Hall bar using photolithography and Ar-ion milling. Subsequently, a lift-off process was used to form Au electrodes to improve the electrical connection with the Co<sub>2</sub>FeSi. We also microfabricated on-chip thermometers consisting of 50-nm-thick Pt wires on the same substrate adjacent to the Co<sub>2</sub>FeSi thin film. (See the Supplemental Material for a photograph of the patterned sample and schematic representation of the experimental configuration.) A homemade holder was used to measure the Seebeck coefficient ( $S_{\text{SE}}$ ) and  $S_{\text{ANE}}$ . The sample was bridged between a Cu heat sink and Cu block, which was thermally connected to a heater to generate a temperature gradient ( $\nabla T$ ) along the thin-film plane. The holder was placed in a Physical Property

Measurement System (PPMS VersaLab; Quantum Design) to control the temperature ( $T$ ) and magnetic field ( $H$ ). To accurately measure  $\nabla T$ , the resistance of the on-chip thermometers was measured using a four-terminal method. A source meter applied 10  $\mu\text{A}$  through two thermometers, while two nanovoltmeters measured the voltages to determine their resistance. Before applying power to the heater and creating  $\nabla T$  along the thin-film plane, we calibrated the on-chip thermometers by measuring their resistance as a function of  $T$  under zero  $H$ . Then, during the measurements of the  $H$  dependence of the thermoelectric signals, we also measured the thermometers when  $H$  was zero. These resistance values were then converted to  $T$  values. The difference in the  $T$  values of the two thermometers was divided by their separation (4 mm) to obtain the value of  $\nabla T$ , while their average was used as the temperature for the obtained  $S_{\text{ANE}}$  and  $S_{\text{SE}}$ . This measurement configuration was used in a previous study [49]. The longitudinal and transverse resistivities of Co<sub>2</sub>FeSi were measured using four-terminal sensing with a standard resistivity puck while varying the value of  $H$  applied along the out-of-plane direction. The AMR of Co<sub>2</sub>FeSi was measured using four-terminal sensing with a rotator, where a  $\mu_0 H$  value of 0.3 T was applied in the thin-film plane.

For first-principles calculations, we first obtained the electronic structure of  $L2_1$ -ordered Co<sub>2</sub>FeSi on the basis of the density-functional theory, including the spin-orbit interaction, which was implemented in the Vienna *ab initio* simulation program (VASP) [50]. We adopted the generalized gradient approximation (GGA) [51] for the exchange-correlation energy and used the projected augmented wave (PAW) pseudo-potential [52,53] to properly treat the effect of core electrons. The lattice constant of the cubic unit cell was fixed at 5.64 Å, as determined from the diffraction peak position observed in the XRD measurement. Because the previous experimental results agreed with the calculations without considering  $U$  at the Fe site [38],  $U$  was considered only for the Co site and was varied from 0 to 3 eV. Using the obtained electronic structure, we calculated  $\sigma_{xy}$  as follows [54]:

$$\sigma_{xy}(\epsilon) = -\frac{e^2}{\hbar} \int \frac{d^3k}{(2\pi)^3} \Omega^z(\mathbf{k}),$$

$$\Omega^z(\mathbf{k}) = -\left(\frac{\hbar}{m}\right)^2 \sum_n f(E_{n,\mathbf{k}}, \epsilon) \sum_{n' \neq n} \frac{2\text{Im}\langle \psi_{n,\mathbf{k}} | p_x | \psi_{n',\mathbf{k}} \rangle \langle \psi_{n',\mathbf{k}} | p_y | \psi_{n,\mathbf{k}} \rangle}{(E_{n',\mathbf{k}} - E_{n,\mathbf{k}})^2},$$

where  $\Omega^z(\mathbf{k})$  is the Berry curvature. Here,  $p_x$  ( $p_y$ ) is the  $x$  ( $y$ ) component of the momentum operator,  $n$  and  $n'$  are the band indices,  $\psi_{n,\mathbf{k}}$  is the eigenstate with eigenenergy  $E_{n,\mathbf{k}}$ , and  $f(E_{n,\mathbf{k}}, \epsilon)$  is the Fermi distribution function for band  $n$  and wave vector  $\mathbf{k}$  at energy  $\epsilon$  relative to  $E_F$ . In the calculation of  $\sigma_{xy}$ , the direction of the magnetization was set to be along the [001]

direction and  $91 \times 91 \times 91$   $k$  points were used for the Brillouin zone integration to ensure good convergence for  $\sigma_{xy}$ . On the basis of the Boltzmann transport theory, we calculated the transverse thermoelectric conductivity,  $\alpha_{xy}$ , for a given temperature  $T$  by using the obtained  $\sigma_{xy}$  in the following expression:

$$\alpha_{xy} = -\frac{1}{eT} \int d\epsilon \left( -\frac{\partial f}{\partial \epsilon} \right) (\epsilon - \mu) \sigma_{xy}(\epsilon),$$

where  $f = 1/[\exp((\epsilon - \mu)/k_B T) + 1]$  is the Fermi distribution function, with  $\mu$  being the chemical potential. Here,  $\mu = 0$  corresponds to  $E_F$ . All of these calculations were also conducted for  $(\text{Co}_{0.95}\text{Fe}_{0.05})_2\text{FeSi}$  with the  $L_{21}$  order to theoretically consider the effect of the off-stoichiometry of the prepared  $\text{Co}_2\text{FeSi}$  thin film on  $\sigma_{xy}$  and  $\alpha_{xy}$ . This treatment is supported by a previous study on  $\text{Co}_2\text{FeGa}_{0.5}\text{Ge}_{0.5}$ , which showed that the potential energy barrier for Fe atoms to occupy Co sites and form Co-Fe disorder is lower than that for Ga or Ge [55]. Here, we used the virtual crystal approximation [56] to treat the mixing between Co and Fe in atomic sites, which was exploited in a previous study to calculate the  $\sigma_{xy}$  and  $\alpha_{xy}$  values of  $\text{Co}_3\text{In}_x\text{Sn}_{2-x}\text{S}_2$  [57].

### 3. Results and discussion

The out-of-plane XRD pattern of the  $\text{Co}_2\text{FeSi}$  thin film is shown in Figure 1(a). Other than the diffraction peaks from the MgO substrate, which are labeled with \*, only the 002 and 004 peaks of  $\text{Co}_2\text{FeSi}$  are

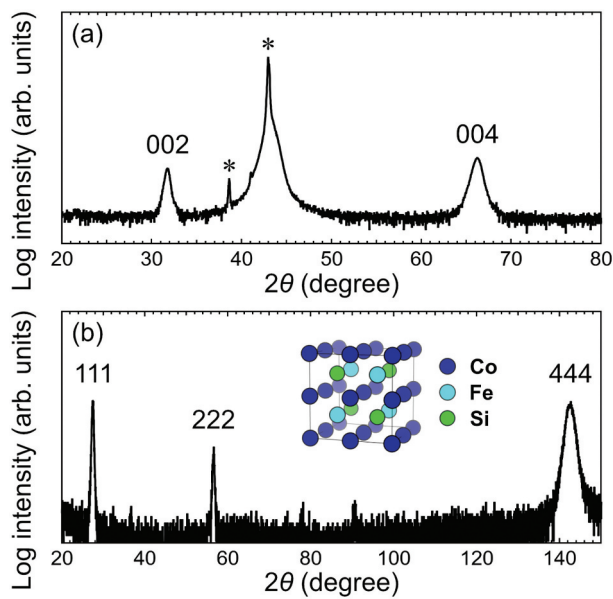


**Figure 1.** (a) Out-of-plane XRD pattern of the  $\text{Co}_2\text{FeSi}$  thin film, showing the 002 and 004 diffraction peaks of  $\text{Co}_2\text{FeSi}$ . The diffraction peaks labeled by \* are from the MgO substrate. (b) XRD pattern measured with the film normal tilted out of the X-ray plane by  $54.7^\circ$ . The 111, 222, and 444 diffraction peaks of  $\text{Co}_2\text{FeSi}$  can be observed. The inset of (b) shows the structure of  $L_{21}$ -ordered  $\text{Co}_2\text{FeSi}$ .

visible. The clear 002 superlattice peak suggested the formation of a B2 structure. To confirm the  $L_{21}$  structure, we obtained the XRD pattern with the film normal tilted out of the X-ray plane by  $54.7^\circ$ , as shown in Figure 1(b). The clear 111 superlattice peak confirmed the existence of the  $L_{21}$  structure, whereas the appearance of diffraction peaks from only the  $\{111\}$  planes indicated the epitaxial growth of  $\text{Co}_2\text{FeSi}$ . The lattice constant of the  $\text{Co}_2\text{FeSi}$  thin film was determined to be  $5.64 \text{ \AA}$  based on XRD measurements, which resulted in a lattice mismatch of approximately 5% with the MgO substrate. Such a lattice mismatch typically induces strain at the  $\text{Co}_2\text{FeSi}/\text{MgO}$  interface, leading to defect formation in the interfacial layer of  $\text{Co}_2\text{FeSi}$ , which would relax the strain. However, because the  $\text{Co}_2\text{FeSi}$  had a thickness of  $41.7 \text{ nm}$ , which was much thicker than the strained interfacial layer of  $\text{Co}_2\text{FeSi}$ , we expected the overall impact of the strain on the thin-film properties to be small. To evaluate the ordering parameters of the B2 and  $L_{21}$  structures, the integrated intensity ratios between the 002 and 004 peaks ( $I_{002}^{\text{exp}}/I_{004}^{\text{exp}}$ ), and between the 111 and 444 peaks ( $I_{111}^{\text{exp}}/I_{444}^{\text{exp}}$ ), were extracted. These values were compared with the simulated intensity ratios ( $I_{002}^{\text{sim}}/I_{004}^{\text{sim}}$  and  $I_{111}^{\text{sim}}/I_{444}^{\text{sim}}$ ) of  $L_{21}$ -ordered  $\text{Co}_2\text{FeSi}$ , which were calculated using the Visualization for Electronic and Structural Analysis (VESTA) software [58], with the actual composition of the thin film taken into consideration. The degree of B2 order ( $S_{B2} = \sqrt{(I_{002}^{\text{exp}}/I_{004}^{\text{exp}})/(I_{002}^{\text{sim}}/I_{004}^{\text{sim}})})$  was estimated to be 1.17, whereas the degree of  $L_{21}$  order ( $S_{L21} = \sqrt{(I_{111}^{\text{exp}}/I_{444}^{\text{exp}})/(I_{111}^{\text{sim}}/I_{444}^{\text{sim}})})$  was estimated to be 0.61. These values are comparable to the ordering parameters reported for  $\text{Co}_2\text{FeSi}$  thin films in previous studies [37,38], indicating that the thin film primarily possessed the  $L_{21}$  structure. Meanwhile, some disorder existed in the thin film, which could have influenced the transport properties of  $\text{Co}_2\text{FeSi}$ . We also measured the in-plane and out-of-plane  $M$ - $H$  curves of  $\text{Co}_2\text{FeSi}$  at 10, 100, 200, and 300 K (see the Supplemental Material). The saturation magnetization ( $M_s$ ) of  $\text{Co}_2\text{FeSi}$  increased slightly with decreasing  $T$ . At 10 K,  $\mu_0 M_s = 1.1 \text{ T}$ , which corresponded to a magnetic moment of  $\sim 4.2 \mu_B/\text{f.u.}$  This value was smaller than the value of  $6 \mu_B/\text{f.u.}$  expected for half-metallic  $\text{Co}_2\text{FeSi}$  at 0 K. As will be shown later, the  $\text{Co}_2\text{FeSi}$  thin film did not exhibit strong half-metallicity; instead, its  $E_F$  was close to the CB edge. Hence, we expect some deviation in the magnetic moment. In addition, the  $\text{Co}_2\text{FeSi}$  thin film was deposited directly on an MgO substrate without a buffer layer, and the lattice mismatch between them could lead to the formation of defects and a magnetic dead layer at the  $\text{Co}_2\text{FeSi}/\text{MgO}$  interface. However, the cause of this reduction in magnetic moment is unclear. Notably, the value of

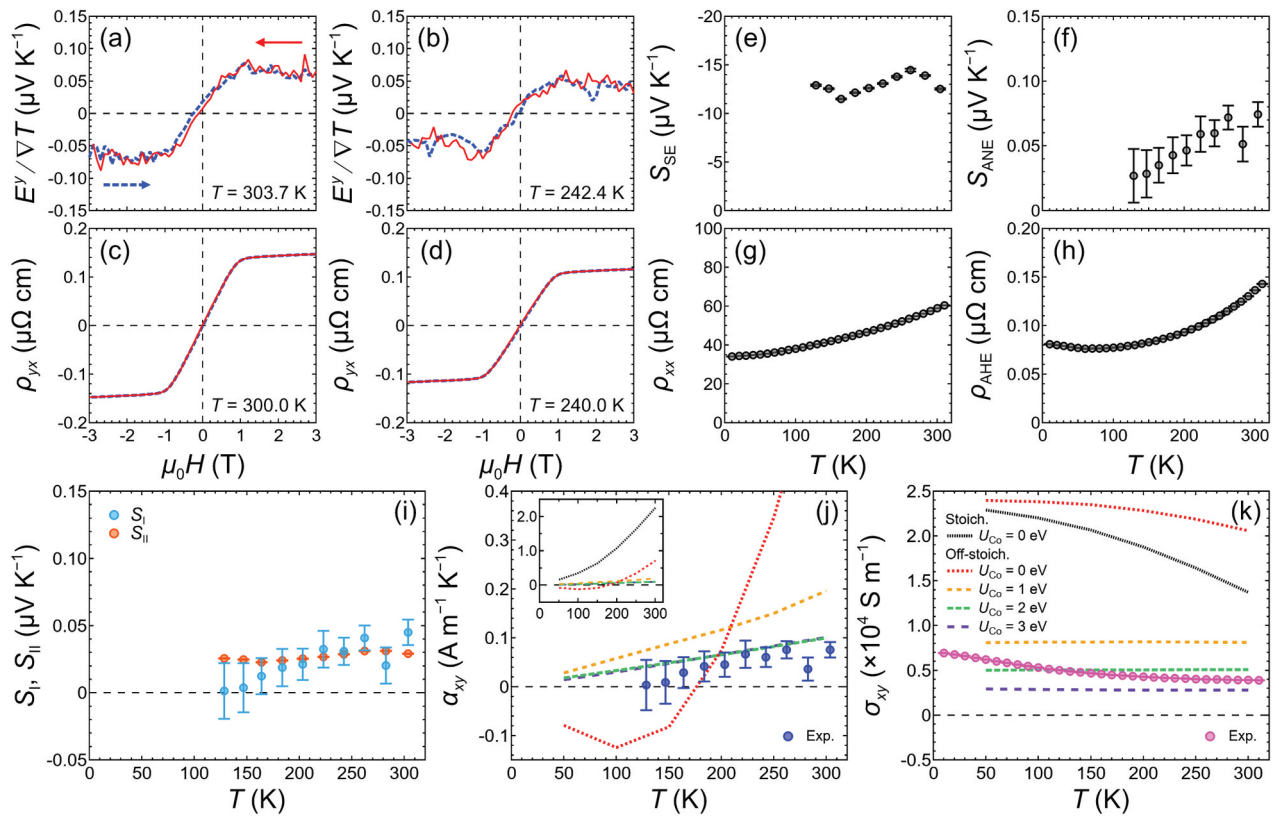
$M_s$  was comparable to some previously reported values obtained using thin films [8,59,60].

Figure 2(a,b) shows the  $H$  dependence of  $E^y/\nabla T$  measured at  $T = 303.7$  and  $242.4$  K, respectively, exhibiting the ANE of the  $\text{Co}_2\text{FeSi}$  thin film. These curves are the average of three measurement loops, each obtained with  $\mu_0 H$  applied along the out-of-plane direction and swept from  $+3$  T to  $-3$  T and then back to  $+3$  T. Here,  $T$  is the estimated temperature of  $\text{Co}_2\text{FeSi}$  corresponding to that of the electrodes used to measure  $E^y$ , which was calculated using the results of two on-chip thermometers while assuming a linear change in  $T$  along the thin-film plane. The curves show  $H$ -odd dependence and saturation at  $|\mu_0 H| \sim 1$  T. Meanwhile, a similar behavior was observed in the  $H$  dependence of  $\rho_{yx}$  (Figure 2(c,d)), exhibiting the AHE of  $\text{Co}_2\text{FeSi}$ . It is worth mentioning that the  $H$  dependence of the ANE and AHE was consistent with the out-of-plane  $M$ - $H$  curve of the  $\text{Co}_2\text{FeSi}$  thin film (see the Supplemental Material). We evaluated  $S_{\text{ANE}}$  and  $\rho_{\text{AHE}}$  of  $\text{Co}_2\text{FeSi}$  by extrapolating the curves at high  $H$  values after saturation down to zero  $H$ . The  $T$  dependences of  $S_{\text{ANE}}$  and  $\rho_{\text{AHE}}$  are shown in

Figure 2(f,h), respectively. The value of  $S_{\text{ANE}}$  was positive but small (less than  $0.1 \mu\text{V K}^{-1}$ ) and decreased with  $T$  within the range of our thermoelectric measurements ( $110.9$ – $303.7$  K). We were able to separate the different components of ANE and evaluate  $\alpha_{xy}$  using the following expression:

$$S_{\text{ANE}} = S_{\text{I}} + S_{\text{II}} = \rho_{xx} \alpha_{xy} - S_{\text{SE}} \frac{\rho_{\text{AHE}}}{\rho_{xx}},$$

along with the measured  $S_{\text{SE}}$  (Figure 2(e)) and longitudinal resistivity ( $\rho_{xx}$ ) (Figure 2(g)) under zero  $H$ . Notably, we calculated  $\rho_{xx}$  and  $\rho_{\text{AHE}}$  at the corresponding  $T$  to match the data for  $S_{\text{SE}}$  and  $S_{\text{ANE}}$  by assuming a linear interpolation between adjacent data points with a spacing of  $10$  K. As shown in Figure 2(i), the  $S_{\text{I}}$  term, in which  $\alpha_{xy}$  played a crucial role, followed the trend of the  $T$  dependence of  $S_{\text{ANE}}$  and decreased as  $T$  decreased towards zero. By contrast, the  $S_{\text{II}}$  term, which was due to the AHE acting on the longitudinal charge current induced by the SE, showed minimal  $T$  dependence. Overall, the  $S_{\text{I}}$  and  $S_{\text{II}}$  terms were comparable in magnitude. Figure 2(j) shows  $\alpha_{xy}$  as a function of  $T$ . The value of  $\alpha_{xy}$  was less than  $0.1$



**Figure 2.** (a) Magnetic field  $H$  dependence of transverse thermal power ( $E^y/\nabla T$ ) of the  $\text{Co}_2\text{FeSi}$  thin film measured at  $T = 303.7$  and (b)  $242.4$  K, exhibiting the ANE of  $\text{Co}_2\text{FeSi}$ . (c)  $H$  dependence of  $\rho_{yx}$  value of  $\text{Co}_2\text{FeSi}$  measured at  $300.0$  K and (d)  $240.0$  K, exhibiting the AHE of  $\text{Co}_2\text{FeSi}$ . (e) The measured  $S_{\text{SE}}$ , (f)  $S_{\text{ANE}}$ , (g)  $\rho_{xx}$ , and (h)  $\rho_{\text{AHE}}$  values of  $\text{Co}_2\text{FeSi}$  as functions of  $T$ , summarizing the  $T$  dependences of its transport properties. (i)  $T$  dependence of the  $S_{\text{I}}$  and  $S_{\text{II}}$  terms, which together constitute the ANE of  $\text{Co}_2\text{FeSi}$ . (j)  $\alpha_{xy}$  and (k)  $\sigma_{xy}$  values of  $\text{Co}_2\text{FeSi}$  as functions of  $T$  measured in the experiment, in comparison with the calculated results for stoichiometric (Stoich.) and off-stoichiometric (off-stoich.) compositions with various values for the on-site Coulomb interaction at the Co site ( $U_{\text{Co}}$ ). The results for the off-stoichiometric composition were calculated using a unit cell of  $(\text{Co}_{0.95}\text{Fe}_{0.05})_2\text{FeSi}$ , which corresponded to the actual composition of the  $\text{Co}_2\text{FeSi}$  thin film. The inset of (j) shows the calculated results over a wider range of  $-0.5$  to  $+2.5 \text{ A m}^{-1} \text{ K}^{-1}$  for the  $y$ -axis. The legends in (k) for the calculated results also apply to (j).

A  $\text{m}^{-1} \text{K}^{-1}$  at room temperature, and decreased slightly with  $T$ . Comparing to the predicted value of  $2.57 \text{ A m}^{-1} \text{K}^{-1}$  for  $\alpha_{xy}$  at 300 K without considering  $U$  [48], there was a clear discrepancy, as the values obtained in the experiment were more than one order of magnitude smaller. We also obtained the  $\sigma_{xy}$  values of  $\text{Co}_2\text{FeSi}$  using the equation  $\sigma_{xy} = \rho_{\text{AHE}} / (\rho_{xx}^2 + \rho_{\text{AHE}}^2)$ , as shown in Figure 2(k). The obtained values of  $\rho_{xx}$  and  $\rho_{\text{AHE}}$  were consistent with those found in previous studies [61,62].

To gain insight into this discrepancy, we evaluated the  $\sigma_{xy}$  and  $\alpha_{xy}$  values of  $\text{Co}_2\text{FeSi}$  using first-principles calculations. Because the  $\text{Co}_2\text{FeSi}$  thin film used in the experiment contained approximately 10% more Fe than the stoichiometric composition, we first studied the effect of this extra Fe using a unit cell of  $(\text{Co}_{0.95}\text{Fe}_{0.05})_2\text{FeSi}$ . Here, the calculated results for  $(\text{Co}_{0.95}\text{Fe}_{0.05})_2\text{FeSi}$  are referred to as off-stoichiometric in this study. The spin-resolved density of states (DOS) values of the stoichiometric and off-stoichiometric compositions with  $U_{\text{Co}} = 0 \text{ eV}$  are shown in Figure 3(a) for comparison. The CB edge of the minority spin shifted slightly to higher energy for the off-stoichiometric composition. Figure 3(b) (Figure 3(d)) shows the  $\sigma_{xy}$  values of the stoichiometric (off-stoichiometric) composition around  $E_F$  at  $T$  values ranging from 50 to 300 K in 50 K steps, while the corresponding  $\alpha_{xy}$  values are shown in Figure 3(c) (Figure 3(e)).  $E_F$  crossed the lower energy side of a peak in  $\alpha_{xy}$ , resulting in large values and substantial  $T$  dependences for both cases, as shown in Figure 3(c, e). The  $T$  dependences of  $\alpha_{xy}$  and  $\sigma_{xy}$  at  $E_F$  are plotted in Figure 2(j, k), respectively, in comparison to the experimental results. For the stoichiometric composition,  $\alpha_{xy} = 2.3 \text{ A m}^{-1} \text{K}^{-1}$  at 300 K (inset of Figure 2(j)), which was similar to the value predicted in a previous study [48]. After taking the composition into consideration,  $\alpha_{xy}$  exhibited a clear decrease to  $0.7 \text{ A m}^{-1} \text{K}^{-1}$  at 300 K for the off-stoichiometric composition, although it was still one order of magnitude larger than the  $\alpha_{xy}$  value obtained in the experiment. We then considered the effect of  $U_{\text{Co}}$ , and performed first-principles calculations for  $\text{Co}_2\text{FeSi}$  with  $U_{\text{Co}} = 1, 2$ , and  $3 \text{ eV}$ . The spin-resolved DOS values of the off-stoichiometric composition with various  $U_{\text{Co}}$  values are summarized in Figure 3(a) as well. The CB edge of the minority spin exhibited a substantial shift toward higher energy with increasing  $U_{\text{Co}}$ .  $E_F$  lay in the middle of the bandgap in the minority-spin channel when  $U_{\text{Co}} = 3 \text{ eV}$ , exhibiting strong half-metallicity, which agreed with previously calculated results [26]. Figure 3(f–k) shows  $\sigma_{xy}$  and  $\alpha_{xy}$  values around  $E_F$  at different  $T$  values for the off-stoichiometric composition with finite  $U_{\text{Co}}$ . Compared to the case with zero  $U_{\text{Co}}$ , the peak responsible for large  $\alpha_{xy}$  also shifted to higher energy with increasing  $U_{\text{Co}}$ . Consequently, the  $\alpha_{xy}$  values at  $E_F$

further decreased to close to zero and exhibited minimal  $T$  dependence, as shown in Figure 2(j). The calculated  $\alpha_{xy}$  values agreed well with the experimental results especially when  $U_{\text{Co}} > 1 \text{ eV}$ . Meanwhile, the values of  $\sigma_{xy}$  obtained in the experiment were closer to the calculated results when a finite  $U_{\text{Co}}$  was considered, as shown in Figure 2(k). However, the trend of a slight decrease in  $\sigma_{xy}$  with increasing  $T$  observed in the experiment was not reproduced in the calculation. Notably, the calculated  $\alpha_{xy}$  only accounted for the intrinsic contribution originating from the Berry curvature. Extrinsic mechanisms, such as skew scattering and side-jump, may have contributed to the  $\alpha_{xy}$  value of the  $\text{Co}_2\text{FeSi}$  thin film in the experiment, although they were not theoretically considered in this study. The temperature dependence of  $\alpha_{xy}$  obtained in the experiment agreed well with the calculated results, suggesting that the ANE of the  $\text{Co}_2\text{FeSi}$  thin film can be explained by the intrinsic contribution of  $\alpha_{xy}$  originated from the Berry curvature. A mostly identical behavior in spin-resolved DOS,  $\sigma_{xy}$ , and  $\alpha_{xy}$  values were observed for the stoichiometric composition with finite  $U_{\text{Co}}$  (see the Supplemental Material). These results suggest that  $U_{\text{Co}}$  should be taken into consideration when describing the  $\sigma_{xy}$  and  $\alpha_{xy}$  values of  $\text{Co}_2\text{FeSi}$ .

As  $U_{\text{Co}}$  increased, the spin-resolved DOS of  $\text{Co}_2\text{FeSi}$  showed an increase in energy for the CB edge, exhibiting a clear bandgap in the minority-spin channel at  $E_F$  (Figure 3(a)). However, this was not supported by experimental observations. We measured the AMR effect using the same sample to study the electronic band structure around  $E_F$  of  $\text{Co}_2\text{FeSi}$ . We applied an electrical current  $I = 1 \text{ mA}$  along the  $[100]$  direction of the  $\text{MgO}$  substrate ( $\parallel [110]$  direction of  $\text{Co}_2\text{FeSi}$ ) and measured the longitudinal resistivity using four-terminal sensing. A  $\mu_0 H$  value of  $0.3 \text{ T}$  was applied within the thin film plane during the measurement, and  $\Phi$  was used to define the direction of  $H$ , where  $\Phi = 0$  indicated that  $H \parallel I$  (inset of Figure 4(a)). In addition to the conventional method of determining the AMR ratio by sweeping  $\Phi$  from  $0^\circ$  to  $360^\circ$  (Figure 4(c)), we also used a different method, *i.e.*, only measuring the longitudinal resistivity at  $\Phi = 0^\circ$  ( $\rho_{\parallel}$ ) and  $\Phi = 90^\circ$  ( $\rho_{\perp}$ ) at different  $T$  values, to obtain the  $T$  dependence of AMR with better detail. The AMR ratio  $\left( = (\rho_{\parallel} - \rho_{\perp}) / \rho_{\perp} \times 100\% \right)$  as a function of  $T$  from 10 to 400 K is shown in Figure 4(a). The results obtained using the conventional method are shown in Figure 4(a) for comparison, where a quantitative agreement can be seen, demonstrating the validity of this method. The AMR ratio was negative at low  $T$ , increased monotonically with increasing  $T$ , and eventually changed sign to positive at  $\sim 377 \text{ K}$ . To further gain insight into the electronic structure of the  $\text{Co}_2\text{FeSi}$  thin film, we calculated the  $T$  dependence of

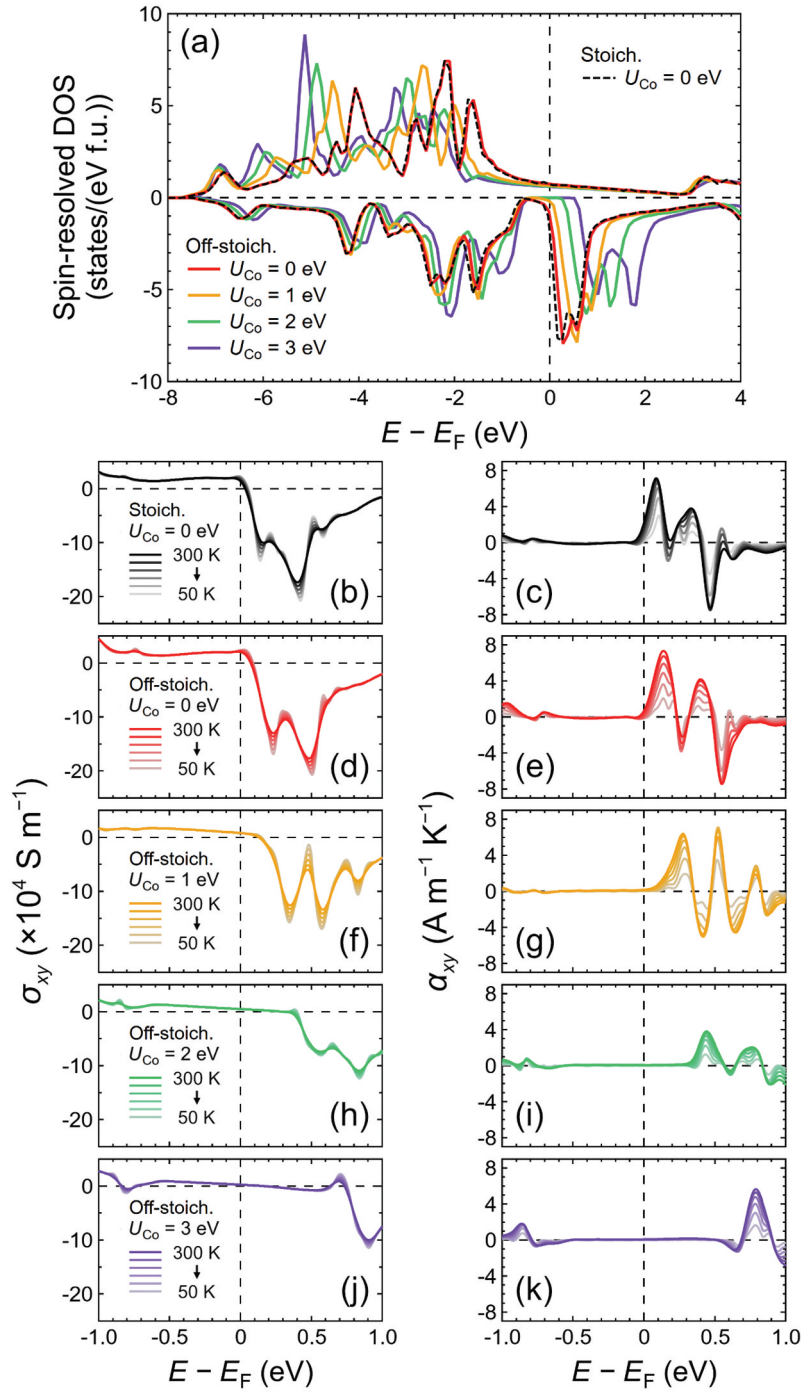


**Figure 3.** (a) Spin-resolved DOS values for  $Co_2FeSi$  with stoichiometric (Stoich.) and off-stoichiometric (off-stoich.) compositions around the Fermi level ( $E_F$ ), with various values for the on-site Coulomb interaction at the Co site ( $U_{Co}$ ). The results for the off-stoichiometric composition were calculated using a unit cell of  $(Co_{0.95}Fe_{0.05})_2FeSi$ , which corresponded to the actual composition of the  $Co_2FeSi$  thin film. (b) Calculated  $\sigma_{xy}$  values of the stoichiometric  $Co_2FeSi$  in the energy window of  $\pm 1$  eV relative to  $E_F$  with  $U_{Co} = 0$  eV, and values of off-stoichiometric  $Co_2FeSi$  with (d)  $U_{Co} = 0$  eV, (f)  $U_{Co} = 1$  eV, (h)  $U_{Co} = 2$  eV, and (j)  $U_{Co} = 3$  eV. (c) Corresponding  $\alpha_{xy}$  values of stoichiometric  $Co_2FeSi$  with  $U_{Co} = 0$  eV, and off-stoichiometric  $Co_2FeSi$  with (e)  $U_{Co} = 0$  eV, (g)  $U_{Co} = 1$  eV, (i)  $U_{Co} = 2$  eV, and (k)  $U_{Co} = 3$  eV. The saturation of colors of the lines indicates the  $T$  values of the results, which ranged from 50 to 300 K in 50 K steps. The values of  $\alpha_{xy}$  and  $\sigma_{xy}$  at  $E_F$  in (b)–(k) as functions of  $T$  are shown in Figure 2(j, k), respectively.

$\Delta\rho = \rho_{\parallel} - \rho_{\perp}$  normalized by the value at 10 K, as shown in Figure 4(b). As seen,  $\Delta\rho$  showed minimal  $T$  dependence from 10 to  $\sim 200$  K, after which it exhibited a clear trend of decreasing in magnitude with increasing  $T$ . Following the modeling of the AMR effect proposed by Kokado et al. [29] and its application to the

AMR effect of the half-metallic Heusler alloy  $Co_2FeGa_{0.5}Ge_{0.5}$  [31],  $\Delta\rho$  can be approximately proportional to  $\rho_{s,\uparrow \rightarrow d,\downarrow} - \rho_{s,\uparrow \rightarrow d,\uparrow}$ , where  $\rho_{s,\uparrow \rightarrow d,\downarrow}$  ( $\rho_{s,\uparrow \rightarrow d,\uparrow}$ ) is the resistivity for the  $s$ - $d$  scattering from the  $s$  electron of  $\uparrow$  spin to the localized  $d$  states of  $\downarrow$  spin ( $\uparrow$  spin). If we ignore the parameters that are

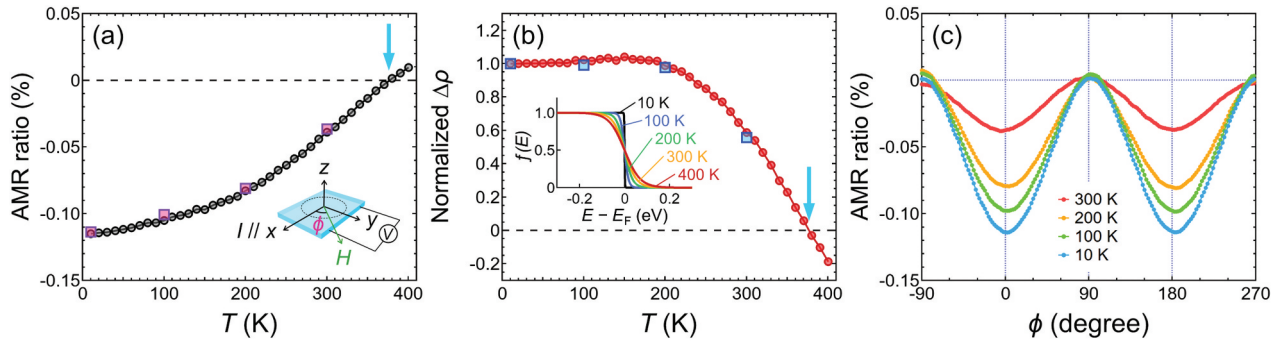


**Figure 4.** (a) AMR ratio  $\left( = (\rho_{\parallel} - \rho_{\perp}) / \rho_{\perp} \times 100\% \right)$  of the  $\text{Co}_2\text{FeSi}$  thin film measured from 10 to 400 K. The inset shows a schematic of the AMR measurement showing the definition of  $\phi$  to represent the direction of  $H$ . (b)  $\Delta\rho$  ( $\rho_{\parallel} - \rho_{\perp}$ ) values of  $\text{Co}_2\text{FeSi}$  normalized by the value at 10 K as a function of  $T$ . The inset illustrates the Fermi distribution function ( $f(E)$ ) at different  $T$  values. The cyan arrows in (a) and (b) mark the sign changes in the AMR ratio and normalized  $\Delta\rho$  at  $T \sim 377$  K. (c) AMR ratio as a function of  $\phi$  measured at various  $T$ . The values obtained from (c) are plotted in (a) and (b) as squares at the corresponding  $T$  for comparison.

negligibly affected by  $T$ ,  $\rho_{s,\uparrow} \rightarrow d_{\downarrow}$  ( $\rho_{s,\uparrow} \rightarrow d_{\uparrow}$ ) can be further simplified to be proportional to  $D_{\downarrow}^{(d)}(E_F)$  ( $D_{\uparrow}^{(d)}(E_F)$ ). Here,  $D_{\downarrow}^{(d)}(E_F)$  ( $D_{\uparrow}^{(d)}(E_F)$ ) represents the DOS of the  $d$  states of  $\downarrow$  spin ( $\uparrow$  spin) around  $E_F$  that contributes to the  $s$ - $d$  scattering, while also having the thermally excited electron occupation following the Fermi distribution function ( $f(E)$ ) taken into consideration (inset of Figure 4(b)). As seen in the case of  $\text{Co}_2\text{FeGa}_{0.5}\text{Ge}_{0.5}$ , the DOS of the  $d$  states of  $\uparrow$  spin is nearly independent of energy around  $E_F$ , and the  $T$  dependence of  $\Delta\rho$  is mainly due to  $D_{\downarrow}^{(d)}(E_F)$ . As a result,  $\Delta\rho$  being independent of  $T$  suggests that  $E_F$  is located around the center of the bandgap in the minority-spin channel; whereas clear decrease in the normalized  $\Delta\rho$  with increasing  $T$  would indicate that  $E_F$  lies close to a band edge that is adjacent to the bandgap, or there are in-gap states formed in the bandgap [31]. In line with this argument, Figure 4(b) suggests that the  $E_F$  of  $\text{Co}_2\text{FeSi}$  lies in the bandgap in the minority-spin channel but is relatively close to the CB edge. For comparison, the CB edge of the minority spin of  $L2_1$ -ordered  $\text{Co}_2\text{FeGa}_{0.5}\text{Ge}_{0.5}$  was estimated to be  $\sim 0.3$  eV above  $E_F$  using first-principles calculations, while its normalized  $\Delta\rho$  showed no decrease with increasing  $T$  up to 300 K [31]. Therefore, the observed  $T$  dependence of the normalized  $\Delta\rho$  of the  $\text{Co}_2\text{FeSi}$  thin film would contradict the CB edge of the minority spin being further away from  $E_F$  than  $\text{Co}_2\text{FeGa}_{0.5}\text{Ge}_{0.5}$ . The calculated spin-resolved DOS with  $U_{\text{Co}}$  values of 2 and 3 eV showed that the CB edge was at approximately 0.3 and 0.6 eV above  $E_F$ , respectively (Figure 3(a)). Thus, the  $T$  dependence of the normalized  $\Delta\rho$  of the AMR effect sets an upper boundary for the  $U_{\text{Co}}$  value of the  $\text{Co}_2\text{FeSi}$  thin film to be smaller than 2 eV. Meanwhile, in comparison with the calculated results, the experimentally measured  $T$  dependence of  $\alpha_{xy}$  sets a lower boundary for the

$U_{\text{Co}}$  value to be larger than 1 eV. Overall, our results suggested that a nonzero but small  $U_{\text{Co}}$  of approximately 1–2 eV is appropriate for describing the transport properties of  $\text{Co}_2\text{FeSi}$ .

#### 4. Conclusions

We systematically studied the transport properties of  $\text{Co}_2\text{FeSi}$  thin films at various  $T$  values. The experimentally measured  $\alpha_{xy}$  values were positive but less than  $0.1 \text{ A m}^{-1} \text{ K}^{-1}$ , and only exhibits a slight decrease with decreasing  $T$ . This led to a small  $S_{\text{ANE}}$  of less than  $0.1 \mu\text{V K}^{-1}$ . This behavior agreed with the theoretical prediction if a  $U_{\text{Co}}$  value larger than 1 eV was considered in the first-principles calculations. On the other hand, the  $T$  dependence of  $\Delta\rho$  due to the AMR effect suggested that  $E_F$  of  $\text{Co}_2\text{FeSi}$  fell in the bandgap in the minority-spin channel but was close to the CB edge. This contradicted the theoretical prediction when a  $U_{\text{Co}}$  value of 2 eV or higher was incorporated in the calculations. Therefore, a  $U_{\text{Co}}$  value of approximately 1–2 eV was found to be appropriate to explain the experimental results. Our findings demonstrated that measuring the  $T$  dependence of the anomalous Nernst conductivity and anisotropic magnetoresistance could be a powerful tool for studying the electronic band structure close to  $E_F$  and probing the effect of on-site Coulomb interaction. In addition, our results suggest that the effect of on-site Coulomb interaction should be examined when calculating the electronic band structure and transport properties of Co-based Heusler alloys.

#### Acknowledgments

The authors thank Y. Miura and A. Yasui for their valuable discussions.

## Disclosure statement

No potential conflict of interest was reported by the author(s).

## Funding

This work was supported by JST ERATO “Magnetic Thermal Management Materials” [Grant No. JPMJER2201], JST CREST “Exploring Innovative Materials in Unknown Search Space” [Grant No. JPMJCR21O1], and JSPS KAKENHI [Grant No. JP25H00743, JP24K00932, JP23K03934, JP22K20494, and JP17H06152]. The synchrotron radiation experiments were performed at the BL09XU of SPring-8 with the approval of the Japan Synchrotron Radiation Research Institute (JASRI) (Proposal No. 2021B1468).

## ORCID

Weinan Zhou  <http://orcid.org/0000-0003-2946-9913>  
 Keisuke Masuda  <http://orcid.org/0000-0002-6884-6390>  
 Kazuki Sumida  <http://orcid.org/0000-0002-5783-3703>  
 Yuichi Fujita  <http://orcid.org/0000-0002-1798-1066>  
 Akio Kimura  <http://orcid.org/0000-0002-1501-3918>  
 Yuya Sakuraba  <http://orcid.org/0000-0003-4618-9550>

## References

- [1] Brown PJ, Neumann KU, Webster PJ, et al. The magnetization distributions in some Heusler alloys proposed as half-metallic ferromagnets. *J Phys Condens Matter*. 2000;12:1827. doi: 10.1088/0953-8984/12/8/325
- [2] Picozzi S, Continenza A, Freeman AJ. Co<sub>2</sub>MnX (X = Si, Ge, Sn) Heusler compounds: an *Ab initio* study of their structural, electronic, and magnetic properties at zero and elevated pressure. *Phys Rev B*. 2002;66(9):094421. doi: 10.1103/PhysRevB.66.094421
- [3] Galanakis I, Dederichs PH, Papanikolaou N. Slater-Pauling behavior and origin of the half-metallicity of the full-Heusler alloys. *Phys Rev B*. 2002;66(17):174429. doi: 10.1103/PhysRevB.66.174429
- [4] Kübler J, Fecher GH, Felser C. Understanding the trend in the Curie temperatures of Co<sub>2</sub>-based Heusler compounds: *Ab initio* calculations. *Phys Rev B*. 2007;76(2):024414. doi: 10.1103/PhysRevB.76.024414
- [5] Kandpal HC, Fecher GH, Felser C. Calculated electronic and magnetic properties of the half-metallic, transition metal based Heusler compounds. *J Phys D Appl Phys*. 2007;40(6):1507. doi: 10.1088/0022-3727/40/6/S01
- [6] Sakuraba Y, Hattori M, Oogane M, et al. Giant tunneling magnetoresistance in Co<sub>2</sub>MnSi/Al–O/Co<sub>2</sub>MnSi magnetic tunnel junctions. *Appl Phys Lett*. 2006;88(19):192508. doi: 10.1063/1.2202724
- [7] Li S, Takahashi YK, Furubayashi T, et al. Enhancement of giant magnetoresistance by L<sub>21</sub> ordering in Co<sub>2</sub>Fe(Ge<sub>0.5</sub>Ga<sub>0.5</sub>) Heusler alloy current-perpendicular-to-plane pseudo spin valves. *Appl Phys Lett*. 2013;103(4):042405. doi: 10.1063/1.4816382
- [8] Kimura T, Hashimoto N, Yamada S, et al. Room-temperature generation of giant pure spin currents using epitaxial Co<sub>2</sub>FeSi spin injectors. *NPG Asia Mater*. 2012;4(3):e9. doi: 10.1038/am.2012.16
- [9] Kasahara K, Fujita Y, Yamada S, et al. Greatly enhanced generation efficiency of pure spin currents in Ge using Heusler compound Co<sub>2</sub>FeSi electrodes. *Appl Phys Express*. 2014;7(3):033002. doi: 10.7567/APEX.7.033002
- [10] Inomata K, Ikeda N, Tezuka N, et al. Highly spin-polarized materials and devices for spintronics. *Sci Technol Adv Mater*. 2008;9(1):014101. doi: 10.1088/1468-6996/9/1/014101
- [11] Felser C, Wollmann L, Chadov S, et al. Basics and prospective of magnetic Heusler compounds. *APL Mater*. 2015;3(4):041518. doi: 10.1063/1.4917387
- [12] Elphick K, Frost W, Samiepour M, et al. Heusler alloys for spintronic devices: review on recent development and future perspectives. *Sci Technol Adv Mater*. 2021;22(1):235–271. doi: 10.1080/14686996.2020.1812364
- [13] Kübler J, Felser C. Weyl points in the ferromagnetic Heusler compound Co<sub>2</sub>MnAl. *Europhys Lett*. 2016;114(4):47005. doi: 10.1209/0295-5075/114/47005
- [14] Chang G, Xu SY, Zhou X, et al. Topological Hopf and chain link semimetal states and their application to Co<sub>2</sub>MnGa. *Phys Rev Lett*. 2017;119(15):156401. doi: 10.1103/PhysRevLett.119.156401
- [15] Noky J, Gooth J, Felser C, et al. Characterization of topological band structures away from the Fermi level by the anomalous Nernst effect. *Phys Rev B*. 2018;98(24):241106(R). doi: 10.1103/PhysRevB.98.241106
- [16] Belopolski I, Manna K, Sanchez DS, et al. Discovery of topological Weyl fermion lines and drumhead surface states in a room temperature magnet. *Science*. 2019;365(6459):1278–1281. doi: 10.1126/science.aav2327
- [17] Sumida K, Sakuraba Y, Masuda K, et al. Spin-polarized Weyl cones and giant anomalous Nernst effect in ferromagnetic Heusler films. *Commun Mater*. 2020;1(1):89. doi: 10.1038/s43246-020-00088-w
- [18] Li P, Koo J, Ning W, et al. Giant room temperature anomalous Hall effect and tunable topology in a ferromagnetic topological semimetal Co<sub>2</sub>MnAl. *Nat Commun*. 2020;11(1):3476. doi: 10.1038/s41467-020-17174-9
- [19] Sakai A, Mizuta YP, Nugroho AA, et al. Giant anomalous Nernst effect and quantum-critical scaling in a ferromagnetic semimetal. *Nat Phys*. 2018;14(11):1119. doi: 10.1038/s41567-018-0225-6
- [20] Guin SN, Manna K, Noky J, et al. Anomalous Nernst effect beyond the magnetization scaling relation in the ferromagnetic Heusler compound Co<sub>2</sub>MnGa. *NPG Asia Mater*. 2019;11(1):16. doi: 10.1038/s41427-019-0116-z
- [21] Xu L, Li X, Ding L, et al. Anomalous transverse response of Co<sub>2</sub>MnGa and universality of the room-temperature  $\alpha_{ij}^A/\alpha_{ij}^L$  ratio across topological magnets. *Phys Rev B*. 2020;101(18):180404. doi: 10.1103/PhysRevB.101.180404
- [22] Hu J, Butler T, Cabero ZMA, et al. Regulating the anomalous Hall and Nernst effects in Heusler-based trilayers. *Appl Phys Lett*. 2020;117(6):062405. doi: 10.1063/5.0014879
- [23] Uchida K, Zhou W, Sakuraba Y. Transverse thermoelectric generation using magnetic materials. *Appl Phys Lett*. 2021;118(14):140504. doi: 10.1063/5.0046877

- [24] Nakatani T, Kulkarni PD, Suto H, et al. Perspective on nanoscale magnetic sensors using giant anomalous Hall effect in topological magnetic materials for read head application in magnetic recording. *Appl Phys Lett*. 2024;124(7):070501. doi: [10.1063/5.0191974](https://doi.org/10.1063/5.0191974)
- [25] Wurmehl S, Fecher CH, Kandpal HC, et al. Geometric, electronic, and magnetic structure of  $\text{Co}_2\text{FeSi}$ : Curie temperature and magnetic moment measurements and calculations. *Phys Rev B*. 2005;72(18):184434. doi: [10.1103/PhysRevB.72.184434](https://doi.org/10.1103/PhysRevB.72.184434)
- [26] Kandpal HC, Fecher GH, Felser C, et al. Correlation in the transition-metal-based Heusler compounds  $\text{Co}_2\text{MnSi}$  and  $\text{Co}_2\text{FeSi}$ . *Phys Rev B*. 2006;73(9):094422. doi: [10.1103/PhysRevB.73.094422](https://doi.org/10.1103/PhysRevB.73.094422)
- [27] Gercsi Z, Hono K. *Ab initio* predictions for the effect of disorder and quaternary alloying on the half-metallic properties of selected  $\text{Co}_2\text{Fe}$ -based Heusler alloys. *J Phys Condens Matter*. 2007;19(32):326216. doi: [10.1088/0953-8984/19/32/326216](https://doi.org/10.1088/0953-8984/19/32/326216)
- [28] Bombor D, Blum CGF, Volkonskiy O, et al. Half-metallic ferromagnetism with unexpectedly small spin splitting in the Heusler compound  $\text{Co}_2\text{FeSi}$ . *Phys Rev Lett*. 2013;110(6):066601. doi: [10.1103/PhysRevLett.110.066601](https://doi.org/10.1103/PhysRevLett.110.066601)
- [29] Kokado S, Tsunoda M, Harigaya K, et al. Anisotropic magnetoresistance effects in Fe, Co, Ni,  $\text{Fe}_4\text{N}$ , and half-metallic ferromagnet: a systematic analysis. *J Phys Soc Jpn*. 2012;81(2):024705. doi: [10.1143/JPSJ.81.024705](https://doi.org/10.1143/JPSJ.81.024705)
- [30] Sakuraba Y, Kokado S, Hirayama Y, et al. Quantitative analysis of anisotropic magnetoresistance in  $\text{Co}_2\text{MnZ}$  and  $\text{Co}_2\text{FeZ}$  epitaxial thin films: a facile way to investigate spin-polarization in half-metallic Heusler compounds. *Appl Phys Lett*. 2014;104(17):172407. doi: [10.1063/1.4874851](https://doi.org/10.1063/1.4874851)
- [31] Kushwaha VK, Kokado S, Kasai S, et al. Prediction of half-metallic gap formation and Fermi level position in Co-based Heusler alloy epitaxial thin films through anisotropic magnetoresistance effect. *Phys Rev Mater*. 2022;6(6):064411. doi: [10.1103/PhysRevMaterials.6.064411](https://doi.org/10.1103/PhysRevMaterials.6.064411)
- [32] Gercsi Z, Rajanikanth A, Takahashi YK, et al. Spin polarization of  $\text{Co}_2\text{FeSi}$  full-Heusler alloy and tunneling magnetoresistance of its magnetic tunneling junctions. *Appl Phys Lett*. 2006;89(8):082512. doi: [10.1063/1.2338025](https://doi.org/10.1063/1.2338025)
- [33] Karthik SV, Rajanikanth A, Nakatani TM, et al. Effect of Cr substitution for Fe on the spin polarization of  $\text{Co}_2\text{Cr}_x\text{Fe}_{1-x}\text{Si}$  Heusler alloys. *J Appl Phys*. 2007;102(4):043903. doi: [10.1063/1.2769175](https://doi.org/10.1063/1.2769175)
- [34] Makinistian L, Faiz MM, Panguluri RP, et al. On the half-metallicity of  $\text{Co}_2\text{FeSi}$  Heusler alloy: point-contact Andreev reflection spectroscopy and *ab initio* study. *Phys Rev B*. 2013;87(22):220402. doi: [10.1103/PhysRevB.87.220402](https://doi.org/10.1103/PhysRevB.87.220402)
- [35] Huang HL, Tung JC, Guo GY. Anomalous Hall effect and current spin polarization in  $\text{Co}_2\text{FeX}$  Heusler compounds ( $X = \text{Al, Ga, In, Si, Ge, and Sn}$ ): a systematic *Ab initio* study. *Phys Rev B*. 2015;91(13):134409. doi: [10.1103/PhysRevB.91.134409](https://doi.org/10.1103/PhysRevB.91.134409)
- [36] Oogane M, Shinano M, Sakuraba Y, et al. Tunnel magnetoresistance effect in magnetic tunnel junctions using epitaxial  $\text{Co}_2\text{FeSi}$  Heusler alloy electrode. *J Appl Phys*. 2009;105(7):07C903. doi: [10.1063/1.3062814](https://doi.org/10.1063/1.3062814)
- [37] Chen J, Sakuraba Y, Masuda K, et al. Enhancement of  $L_2$  order and spin-polarization in  $\text{Co}_2\text{FeSi}$  thin film by substitution of Fe with Ti. *Appl Phys Lett*. 2017;110(24):242401. doi: [10.1063/1.4985237](https://doi.org/10.1063/1.4985237)
- [38] Sumida K, Fujita Y, Zhou W, et al. Role of on-site Coulomb interactions in the half-metallic Weyl ferromagnet candidate thin-film  $\text{Co}_2\text{FeSi}$ . *Phys Rev B*. 2023;108(24):L241101. doi: [10.1103/PhysRevB.108.L241101](https://doi.org/10.1103/PhysRevB.108.L241101)
- [39] Xiao D, Yao Y, Fang Z, et al. Berry-phase effect in anomalous thermoelectric transport. *Phys Rev Lett*. 2006;97(2):026603. doi: [10.1103/PhysRevLett.97.026603](https://doi.org/10.1103/PhysRevLett.97.026603)
- [40] Guin SN, Vir P, Zhang Y, et al. Zero-field Nernst effect in a ferromagnetic kagome-lattice Weyl-semimetal  $\text{Co}_3\text{Sn}_2\text{S}_2$ . *Adv Mater*. 2019;31(25):1806622. doi: [10.1002/adma.201806622](https://doi.org/10.1002/adma.201806622)
- [41] Ding L, Koo J, Xu L, et al. Intrinsic anomalous Nernst effect amplified by disorder in a half-metallic semimetal. *Phys Rev X*. 2019;9:041061. doi: [10.1103/PhysRevX.9.041061](https://doi.org/10.1103/PhysRevX.9.041061)
- [42] Yang H, You W, Wang J, et al. Giant anomalous Nernst effect in the magnetic Weyl semimetal  $\text{Co}_3\text{Sn}_2\text{S}_2$ . *Phys Rev Mater*. 2020;4(2):024202. doi: [10.1103/PhysRevMaterials.4.024202](https://doi.org/10.1103/PhysRevMaterials.4.024202)
- [43] Wuttke C, Cagliaris F, Sykora S, et al. Berry curvature unravelled by the anomalous Nernst effect in  $\text{Mn}_3\text{Ge}$ . *Phys Rev B*. 2019;100(8):085111. doi: [10.1103/PhysRevB.100.085111](https://doi.org/10.1103/PhysRevB.100.085111)
- [44] Sakuraba Y, Hyodo K, Sakuma A, et al. Giant anomalous Nernst effect in the  $\text{Co}_2\text{MnAl}_{1-x}\text{Si}_x$  Heusler alloy induced by Fermi level tuning and atomic ordering. *Phys Rev B*. 2020;101(13):134407. doi: [10.1103/PhysRevB.101.134407](https://doi.org/10.1103/PhysRevB.101.134407)
- [45] Sakai A, Minami S, Koretsune T, et al. Iron-based binary ferromagnets for transverse thermoelectric conversion. *Nature*. 2020;581(7806):53–57. doi: [10.1038/s41586-020-2230-z](https://doi.org/10.1038/s41586-020-2230-z)
- [46] Asaba T, Ivanov V, Thomas SM, et al. Colossal anomalous Nernst effect in a correlated noncentrosymmetric kagome ferromagnet. *Sci Adv*. 2021;7(13):eabf1467. doi: [10.1126/sciadv.abf1467](https://doi.org/10.1126/sciadv.abf1467)
- [47] Breidenbach AT, Yu H, Peterson TA, et al. Anomalous Nernst and Seebeck coefficients in epitaxial thin film  $\text{Co}_2\text{MnAl}_x\text{Si}_{1-x}$  and  $\text{Co}_2\text{FeAl}$ . *Phys Rev B*. 2022;105(14):144405. doi: [10.1103/PhysRevB.105.144405](https://doi.org/10.1103/PhysRevB.105.144405)
- [48] Noky J, Zhang Y, Gooth J, et al. Giant anomalous Hall and Nernst effect in magnetic cubic Heusler compounds. *npj Comput Mater*. 2020;6(1):77. doi: [10.1038/s41524-020-0342-5](https://doi.org/10.1038/s41524-020-0342-5)
- [49] Zhou W, Miura A, Sakuraba Y, et al. Direct electrical probing of anomalous Nernst conductivity. *Phys Rev Appl*. 2023;19(6):064079. doi: [10.1103/PhysRevApplied.19.064079](https://doi.org/10.1103/PhysRevApplied.19.064079)
- [50] Kresse G, Furthmüller J. Efficient iterative schemes for *Ab initio* total-energy calculations using a plane-wave basis set. *Phys Rev B*. 1996;54(16):11169–11186. doi: [10.1103/PhysRevB.54.11169](https://doi.org/10.1103/PhysRevB.54.11169)
- [51] Perdew JP, Burke K, Ernzerhof M. Generalized gradient approximation made simple. *Phys Rev Lett*. 1996;77(18):3865–3868. doi: [10.1103/PhysRevLett.77.3865](https://doi.org/10.1103/PhysRevLett.77.3865)
- [52] Blöchl PE. Projector augmented-wave method. *Phys Rev B*. 1994;50(24):17953–17979. doi: [10.1103/PhysRevB.50.17953](https://doi.org/10.1103/PhysRevB.50.17953)
- [53] Kresse G, Joubert D. From ultrasoft pseudopotentials to the projector augmented-wave method. *Phys Rev B*. 1999;59(3):1758–1775. doi: [10.1103/PhysRevB.59.1758](https://doi.org/10.1103/PhysRevB.59.1758)

- [54] Yao Y, Kleinman L, MacDonald AH, et al. First principles calculation of anomalous Hall conductivity in ferromagnetic bcc Fe. *Phys Rev Lett.* **2004**;92(3):037204. doi: [10.1103/PhysRevLett.92.037204](https://doi.org/10.1103/PhysRevLett.92.037204)
- [55] Goto K, Kumara LSR, Sakuraba Y, et al. Effects of the atomic order on the half-metallic electronic structure in the  $\text{Co}_2\text{Fe}(\text{Ga}_{0.5}\text{Ge}_{0.5})$  Heusler alloy thin film. *Phys Rev Mater.* **2020**;4(11):114406. doi: [10.1103/PhysRevMaterials.4.114406](https://doi.org/10.1103/PhysRevMaterials.4.114406)
- [56] Bellaiche L, Vanderbilt D. Virtual crystal approximation revisited: application to dielectric and piezoelectric properties of perovskites. *Phys Rev B.* **2000**;61(12):7877–7882. doi: [10.1103/PhysRevB.61.7877](https://doi.org/10.1103/PhysRevB.61.7877)
- [57] Yanagi Y, Ikeda J, Fujiwara K, et al. First-principles investigation of magnetic and transport properties in hole-doped shandite compounds  $\text{Co}_3\text{In}_x\text{Sn}_{2-x}\text{S}_2$ . *Phys Rev B.* **2021**;103(20):205112. doi: [10.1103/PhysRevB.103.205112](https://doi.org/10.1103/PhysRevB.103.205112)
- [58] Momma K, Izumi F. *Vesta 3* for three-dimensional visualization of crystal, volumetric and morphology data. *J Appl Crystallogr.* **2011**;44(6):1272–1276. doi: [10.1107/S0021889811038970](https://doi.org/10.1107/S0021889811038970)
- [59] Oogane M, Yilgin R, Shinano M, et al. Magnetic damping constant of  $\text{Co}_2\text{FeSi}$  Heusler alloy thin film. *J Appl Phys.* **2007**;101(9):09J501. doi: [10.1063/1.2709751](https://doi.org/10.1063/1.2709751)
- [60] Schneider H, Herbort C, Jakob G, et al. Structural, magnetic and transport properties of  $\text{Co}_2\text{FeSi}$  Heusler films. *J Phys D Appl Phys.* **2007**;40(6):1548. doi: [10.1088/0022-3727/40/6/S06](https://doi.org/10.1088/0022-3727/40/6/S06)
- [61] Imort IM, Thomas P, Reiss G, et al. Anomalous Hall effect in the Co-based Heusler compounds  $\text{Co}_2\text{FeSi}$  and  $\text{Co}_2\text{FeAl}$ . *J Appl Phys.* **2012**;111(7):07D313. doi: [10.1063/1.3678323](https://doi.org/10.1063/1.3678323)
- [62] Yadav A, Chaudhary S. Effect of growth temperature on the electronic transport and anomalous Hall effect response in co-sputtered  $\text{Co}_2\text{FeSi}$  thin films. *J Appl Phys.* **2015**;118(19):193902. doi: [10.1063/1.4935823](https://doi.org/10.1063/1.4935823)